Eddie Tang LLP Report

eddietang2314@gmail.com

1. Introduction

Green energy is vital in the future of technological advancements and in combating climate change. The hydrogen molecule (H_2) serves as an effective energy source that satisfies the requirement for green energy chiefly from its ability to combust cleanly by only forming water and its high gravimetric energy density. However, hydrogen transportation has its challenges and setbacks. Ammonia (NH_3) is a possible solution since it has a high energy density, is a carrier of H2, and is easier to store at room temperature.

Ammonia is synthesized on a large scale from hydrogen and nitrogen through the Haber-Bosch process. Moreover, since ammonia production requires a large amount of energy to break the nitrogen (N_2) triple bond in the NH_3 synthesis reaction and is characterized by centralized facilities to carry out this process, it accounts for 2% of the global energy consumption.

Current developments[1] in combating these downfalls have found that combining electrochemical cells with tungsten oxynitride rods (WO_xN_y) and plasma-assisted nitrogen synthesis yielded promising results. Its advantages are that it is a distributed method of synthesizing NH_3 by being compact and relatively cheap, it has a higher yield of up to 200% compared to current NH_3 fuel cells, and it can use surplus energy that usually goes to waste, effectively becoming an electrified method in producing NH_3.

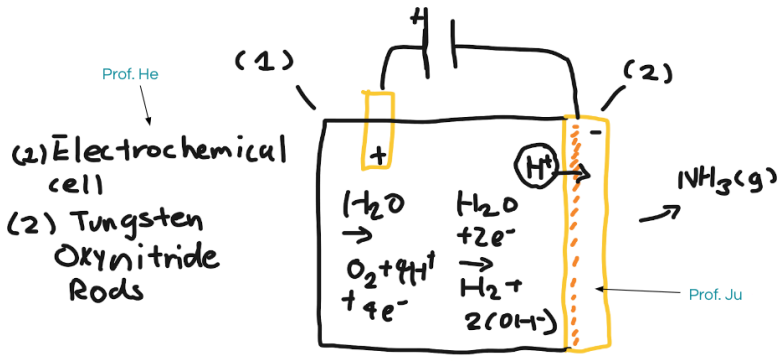

Current Experimental Setup

However, even with experimental results, there is a lack of understanding of the elementary reactions that dictate the many processes in our experiments. Namely, the process of creating WO_xN_y rods by blasting tungsten oxide (WO_3) with hydrogen plasma and then N_2 plasma needs to be better understood from purely experimental analysis, which is the basis of

[1] Our Research Project

question one. Moreover, question two is whether the O-vacancies in the WO_xN_y rods would prefer water (H_2O) or N_2 needs to be clearly understood.

Here, the objective of this project is to investigate and study these elementary reactions through the use of density functional theory (DFT) calculations. These calculations will be used to calculate the absorption energies of H, N_2, H_2O, and H_2 adsorbates to determine chemically and thermodynamically favorable reaction pathways that explain the processes mentioned above.

Lastly, another project that is underway is to study the interaction of nitrogen species and WO_3 surface vacancies through a machine-learned potential energy surface.

2. DFT Methods

2.1. Atomic models

A four-layer WO_3 periodic slab (*S,* 1 × 1) of the lowest-energy surface (001) and a 10 Å vacuum layer on top of the slab surface were generated. Therefore, the optimized supercell dimensions were 7.4984 Å x 7.4984 Å x 27 Å. Calculating the in-plane (α) and out-of-plane (β) angles I get 120° and 90°, respectively. For gaseous species, namely H, N_2, H_2O, and H_2, a 10 Å x 11 Å x 12 Å periodic cubic box was used when sampling their free energies for calculations. Additionally, for simulations not involving vacancies, the adsorbates were placed 1.5 Å above the surface. For simulations involving vacancies, the adsorbates were placed 0.5 Å above the surface.

To generate the initial configurations, a custom Python script[2] was programmed using the Atomic Simulation Environment (ASE) Python package and Pymatgen (Python Materials Genomics). This script can add our gaseous species on top of a set location, generate vacancies on the WO_3 surface, generate gaseous species in the set vacuums, and generate KPOINTS files.

To study the effects further, a 2 × 2 supercell slab was generated with Open Visualization Tool (OVITO) to generate a larger slab (*LS*). This slab has supercell dimensions of 14.9968 Å x 14.9968 Å x 27 Å. Furthermore, *S* was replicated in OVITO once in the y direction to generate a medium slab (*MS,* 1 × 2). This slab has supercell dimensions of 7.498 Å x 14.9968 Å x 27 Å after relaxation.

Both relaxed surfaces were used to study interactions between N_2, H_2O, and O vacancies on the WO_3 surface. Note that this structure is based on the WO_3 hexagonal crystal structure. For WO_3 (001), I used the O-terminated (O_t) side for surface simulations since it is more stable than the W-terminated side.

2.2. Electronic structure theory

DFT calculations were performed using the Vienna Ab-initio Simulation Package (VASP) version 6.3.1. In these calculations, Perdew-Burke-Ernzerhof (PBE) exchange-correlation (XC) functional were used. The wave functions were expanded in a plane wave basis set with a kinetic energy cutoff of 500 eV (ENCUT=500). The Brillouin zone (BZ) was sampled so that the sampling grid preserves the symmetry in the reciprocal space, specifically, for *S*, by 4×4×1, for

[2] https://github.com/EDED2314/VASP-scripts

LS, by 2×2×1, and for *MS*, by 4×2×1 Gamma-centered meshes. The dipole moment will be calculated only parallel to the direction of the third lattice vector in our simulations (IDIPOL=3). Simulations were run involving H adsorbates with spin-polarization to account for the free electrons around H. Other simulations were run without spin-polarization. Forces and stress tensors were calculated to allow the WO_3 structure's position degree of freedom to change (ISIF=2). The Gaussian method was used to smear the electronic states near the Fermi level with a width of 0.05 to aid electronic convergence (ISMEAR=0, SIGMA=0.05). Lastly, van der Waals corrections were not included.

2.3. Structure optimization

A conjugate-gradient algorithm was used for optimization and the self-consistent-field (SCF) threshold was set as 1 meV. I also set the atomic-force component convergence thresholds to 0.01 eV/Å. The bottom two layers of the slab were frozen and the structures were relaxed. Hence, for all adsorbate simulations, I only allowed the top two layers to interact with the adsorbate to simulate a semi-infinite crystal. The calculation factor for the default values for ENCUT (PREC) was set to accurate. Lastly, the maximum number of geometry optimization steps is 100, the maximum number of electronic SC (self-consistency) steps is 100, and the minimum number of electronic SC steps is 10.

2.4. Thermal corrections to the free energy

Since our DFT calculations are done under 0K, I used additional thermal corrections to study the effects of temperature on the WO_3 surface on one H_2O molecule's desorption energy. Typically, the free energy of a gas-phase species is its DFT total internal energy and the sum of translational, vibrational, and rotational vibrations' free energies.[3] Since I am working with slabs, I ignored the translational and rotational vibrations in calculations involving them.

The oxygen terminations, first layer of tungsten, and adsorbate were displaced by 0.015 Å in VASP simulations that do not apply symmetry and calculate the Hessian (IBRION = 5). All of these displacements were performed on optimized structures.

Once the simulation concluded, I used VASPKIT[4] to analyze the vibrational frequencies by deriving the normal mode frequencies from output Hessians in the OUTCAR and outputting free energy corrections for an inputted temperature.

3. DFT Results and Discussion

3.1. The influence of H_2 plasma in oxygen vacancy formation

To investigate the first question regarding how H_2 plasma formed oxygen vacancies, I wanted to calculate the energies of each reaction step to evaluate the chemical favorability of two

[3] Martirez, J. M. P.; Carter, E. A. First-Principles Insights into the Thermocatalytic Cracking of Ammonia-Hydrogen Blends on Fe(110): 1. Thermodynamics. J. Phys. Chem. C 2022, 126 (46), 19733– 19744, doi: 10.1021/acs.jpcc.2c06003

[4] https://vaspkit.com/

hydrogen atoms, or one H_2 molecule to absorb on a surface oxygen atom along the oxygen terminations sites and then desorb from the surface of *S* to form a vacancy and water molecule.

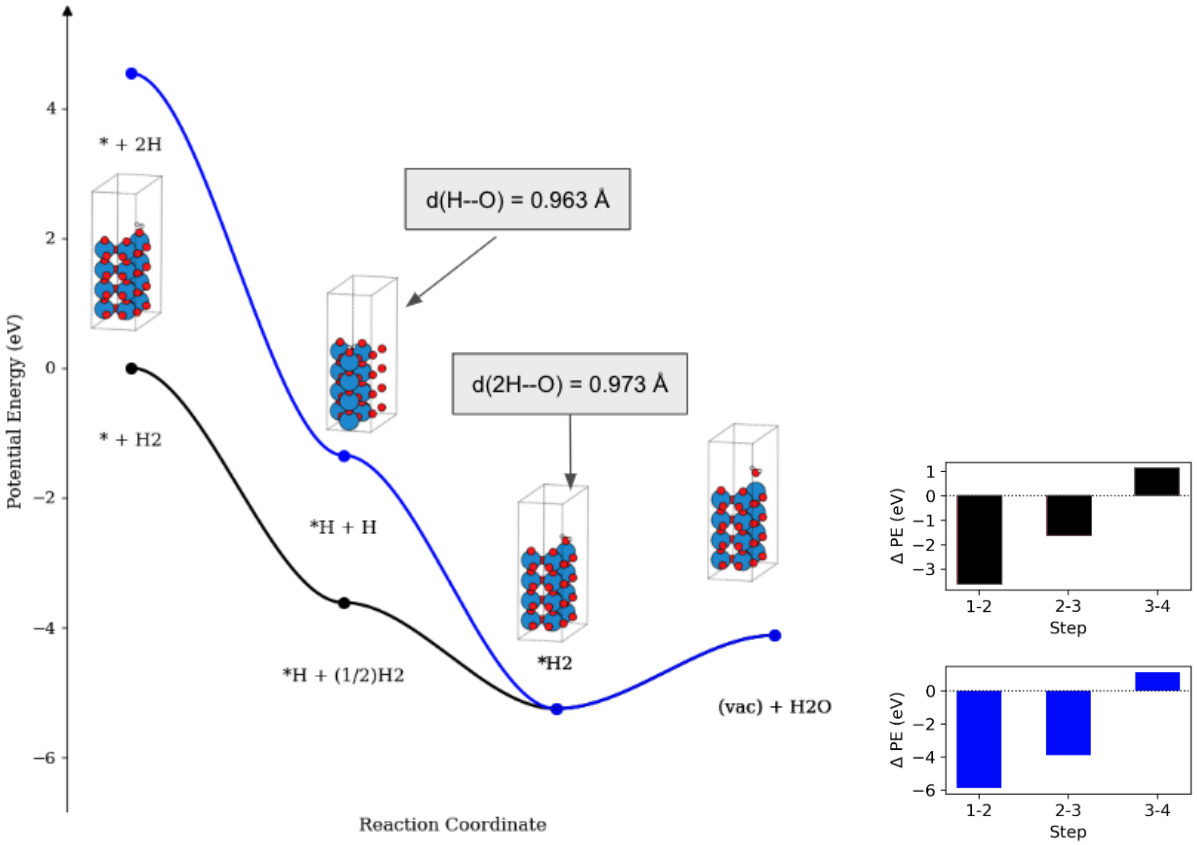

Figure 1. *Left:* Potential surface of surface and H_2 and H reaction at 0 K, *Right*: Potential energy differences between each step.

After verifying the convergence of all structures involved in the specific reaction steps, I extracted the energy of the configurations and plotted them along a potential surface graph in Figure 1 and scaled everything relative to the energy of the surface + H_2. For steps 2 and 3, the bond distance between *H and O_t in the optimized structure is included to indicate a typical hydroxide bond length and water bond length.

Note that the H_2 surface does not include the reaction steps involved in the dissociation of H_2 into two H atoms, which is where we would expect an energy barrier that would require external work to be applied to the system to advance the reaction.

Without including that reaction pathway, we can still infer, from the difference in magnitude of change in potential energy between the reaction steps, that H atoms adsorbing onto O-terminations are more chemically favorable than sourcing *H from H_2. This demonstrates that hydrogen plasma, which gives the system access to individual H atoms, would have more vacancy formation than only H_2 gas.

3.2. H_2O desorption energy barrier

For both pathways in Figure 1, there is a slight uphill (~1 eV) desorption energy of H2O from the surface. Since room temperature, 300K, can only account for 0.03 eV in contribution, other factors could lower this desorption energy barrier. Therefore, I investigated the effects of temperature on this energy barrier and the effects of H_2O coverage concerning this uphill magnitude as well.

3.2.1. Effects of Temperature

I calculated the desorption energies by finding the negative of the adsorption energy. Namely,

$$\Delta E_{desorption} = -\ \Delta E_{ads} = -\ [E_{WO3/X} - (E_{WO3} + E_X)].$$

Where *X* is the adsorbate chemical symbol.

The free energy corrections were then calculated with VASPKIT at a specific temperature and added to the calculated internal potential energy found in VASP outputs to create the table below.

Table 1. Desorption energy calculated with free energy corrected values at corresponding temperatures.

Temperature	H2O Desorption Energy (eV)
0K	1.1285
400K	1.1528
3000K	2.9848

The increasing desorption energies with an increase in temperature do indicate that the reaction step $* H2 \rightarrow H2O + vac$ is slightly exothermic. Additionally, since the final goal of the study is to develop a system that would operate at room temperature, the 3000K serves only as a reference for the desorption energy at higher temperatures. Lastly, the 0.0243eV difference between 0K and 400K indicates that temperature does not significantly affect the desorption temperatures, and hence the amount of vacancies formed.

The vacancy formation energy of *S* is 1.60426 eV and calculated with the equation

$$\Delta E_{vac} = E_{WO3} - (E_{WO3-v} + \frac{1}{2}E_{O2}).$$

This vacancy formation energy is 0.45146 eV greater than the desorption energy of H_2O at 400 K, which suggests that even though H_2O has positive adsorption energy, it is still more energetically favorable to desorb an H_2O molecule than remove an oxygen atom along the surface to form a vacancy. Thus, supporting that H_2 plasma aids in forming O_t vacancies.

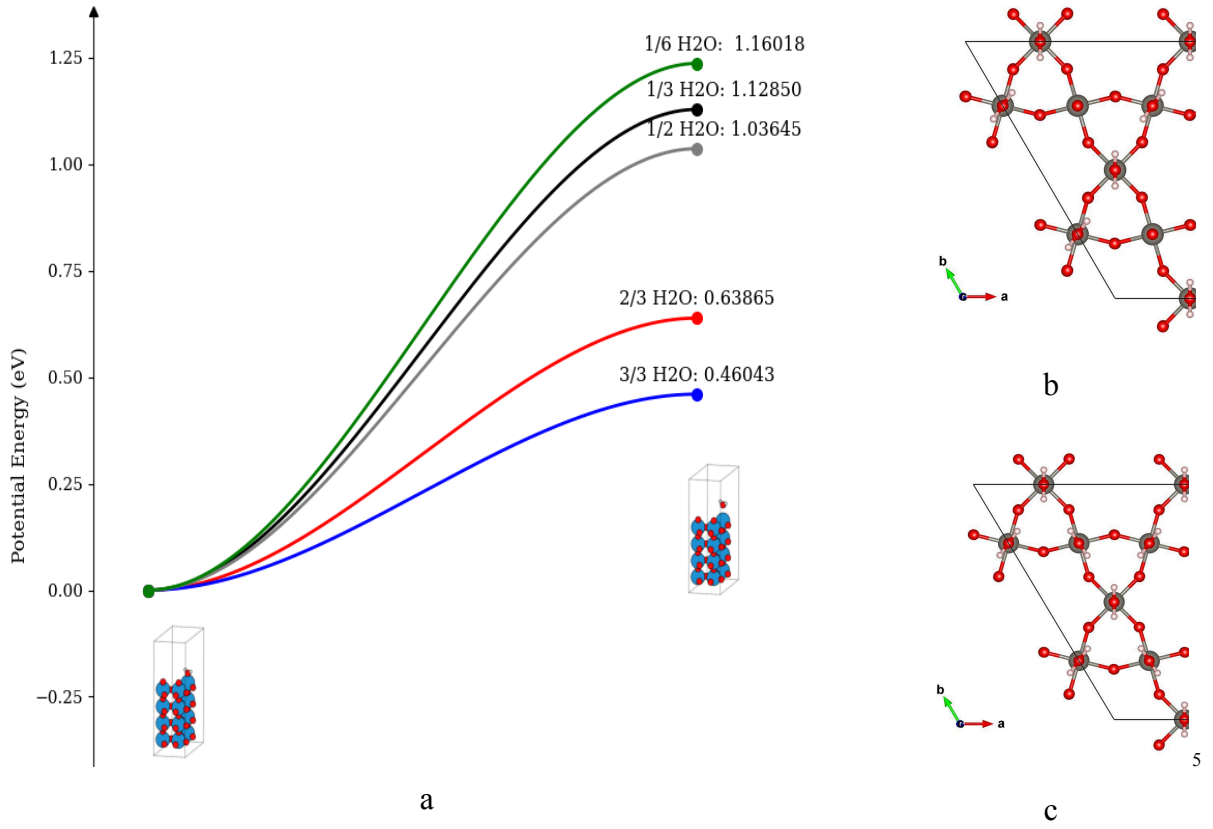

Figure 2. a) Comparison of H_2O desorption energies at different coverage of the O_t sites. b) 3/3 coverage on the 001 surface. c) 2/3 coverage on the 001 surface.

3.2.2. Effects of H_2O Coverage

This study compared the desorption energies of one H_2O molecule with its oxygen facing down at O_t at different adsorbed H_2O coverages to study the effects of H_2O coverage on these sites. Specifically, we conducted the simulations on *S*.

From *Figure 2*, the desorption energy of H_2O at minimal coverage (1/6) is 1.16 eV, which is more than two times the desorption energy of full coverage (3/3) 0.46 eV. There is also decreasing desorption energy as H_2O coverage on the oxygen termination sites increases. Hence, the coverage effects on combating the H_2O desorption energy barrier are non-negligible and significant.

Qualitatively examining these results also yields strengthened confidence, since more water absorbed on the surface will mean many more hydrogen-bond interactions and electron repulsion between the partial-negatives and partial-positives. It is hypothesized that these electron repulsions contribute to the smaller desorption energy.

---

[5] K. Momma and F. Izumi, "VESTA 3 for three-dimensional visualization of crystal, volumetric and morphology data," J. Appl. Crystallogr., 44, 1272-1276 (2011).

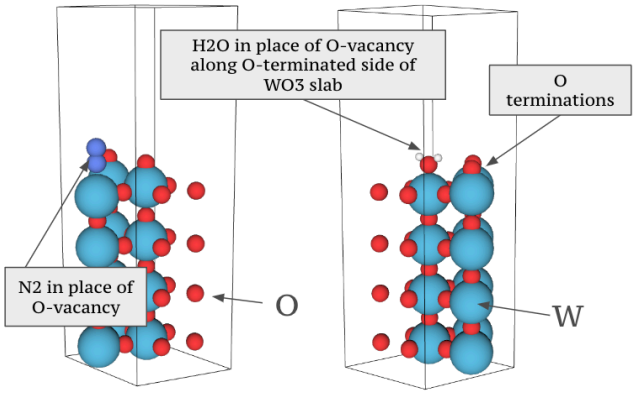

Figure 3. Initial configurations. Left: N_2 on top of O_t vacancy. Right: H_2O on top of O_t vacancy.

Table 2. Calculated adsorption energies of H_2O and N_2 into O_t vacancies.

Adsorbate	Adsorption Energy (eV)
H_2O	-1.1285[6]
N_2	-0.3556

Thus, I hypothesize that as the reaction continues with more atomic H adsorbed onto *H and * to form *H2 (*H_2O + vac) and *H respectively, there would be an increased rate at which vacancies form since the reaction barrier for H_2O desorption decreases with more adsorbed water. Overall, it is clear that higher H_2O coverage will contribute to more vacancies.

3.3. H_2O versus N_2 adsorption onto O_t vacancies

The second question is looked into by simply calculating the adsorption energy of water versus nitrogen at 1/3 coverage on *S* at an O_t vacancy site. The nitrogen molecule in its initial configuration is oriented upright while the water molecule is oriented so that its oxygen atom points downwards into the vacancy.

In *Table 2*, the calculated adsorption energy of H_2O is less than N_2, which means that under conditions listed in the methods, O_t vacancies will prefer water more than nitrogen since the adsorption is more chemically favorable. However, it is necessary to note that accounting for the electrochemical origins of water in the simulation environment may significantly affect these values since the hydrogen bonding may lead water to be less attracted to surface vacancies. Additionally, the water adsorption energy may decrease due to coverage effects, which have not been tested yet.

These results reveal that future experimental setups may find it more difficult to treat WO_3 with N_2 plasma to obtain WO_xN_y (x+y < 3) or W_xN_y.

[6] This result is similar to hexagonal calculations done by other literature, where the adsorption energy of H_2O is -1.22 eV.

3.4. Additional results

3.4.1. Spin-Polarized Calculations

I have attached below the spin-polarized calculations. They yield significantly different results, which may be due to the electrons within the WO2 structure itself being fully accounted for in the spin-polarized calculations.

Adsorption/desorption (for H2O) energies

	SP	no SP
n-o	-6.300231	-7.352501
no-vac	-0.839013	-1.777893
n2-o	-1.521460	-1.624960
n2o-vac	-0.209161	-0.199271
n2-bridge0	-0.030220	-0.032640
h-O0	-4.743186	-5.883536
n-vac	-0.264831	-1.171646
n2-vac	-0.364560	-0.355680
h2o 1/3	1.134578	1.128501
h2o 2/3	0.405528	0.638658
h2o 3/3	0.055608	0.460138
vac_form	1.490868	1.604258

Energy of systems, and comparison to whether SP decreased it.

	SP	no SP	SP < no SP?
wo3 energy	-349.51698	-348.464710	True
wo3 v energy	-346.06652	-345.127640	True
2 h2o 1 vac energy	-355.52345	-354.450970	True
3 h2o 1 vac energy	-362.21825	-360.323120	True
1 h2o energy	-361.43218	-360.487223	True
2 h2o energy	-370.16006	-369.320710	True
3 h2o energy	-376.50494	-375.014340	True
n o0 energy	-358.94094	-358.940940	False
n2 o0 energy	-367.68835	-366.739580	True
n2 bridge0 energy	-366.19711	-365.147260	True
h energy	-355.37725	-355.465330	False
n vac energy	-349.45508	-349.423015	True
n2 vac energy	-363.08099	-362.133230	True

3.4.2. Effect of N_2 coverage on N_2 adsorption energies

Since the nitrogen adsorption energy was more than two times less than the water adsorption energy into an O_t vacancy, a few additional simulations were run to compare coverage and adsorption energy.

The adsorption energy for N_2 is calculated with

$$\Delta E_{ads\ N2} = E_{WO3(vac)/N2} - (E_{WO3(vac)} + E_{N2}).$$

Table 3. N_2 coverage on 001 surface above O_t vacancies versus adsorption energy.

Coverage	Adsorption Energy (eV)
1/3	-0.3556
1/12	-0.3964

It is found that with fewer adsorbates, it is more chemically favorable for N_2 to adsorb onto a vacancy since 1/12 adsorption energy is less than 1/3. However, the difference of 0.0408 eV indicates that the coverage effects for N_2 are less significant than H_2O.

3.4.3. Nitrogen species adsorption investigation

In addition to N_2 versus H_2O adsorption into O_t vacancies, I investigated N and N_2 adsorption onto O_t and a bridge oxygen atom (O_b), NO, and N_2O adsorption into O_t vacancies.

All these species were placed in their upright orientations for initial structures on *S*. The motivation is to investigate pathways nitrogen species may take during N_2 plasma treatment.

Table 4. **Adsorption energies of different nitrogen species**

Location	Adsorbate	Adsorption Energy (eV)
O_t	N	-7.353
O_t	N_2	-1.777
$O_{t\text{-}v}$	NO	-1.625
$O_{t\text{-}v}$	N_2O	-0.199
O_b	N_2	-0.356

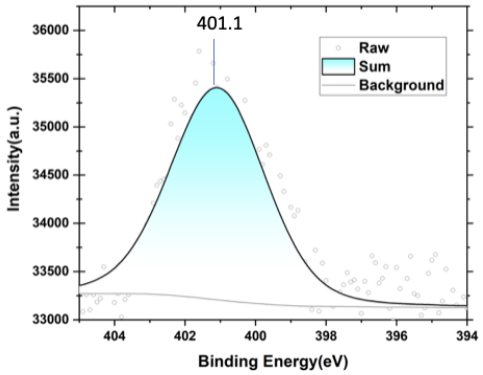

Figure 4. N 1s XPS plot on N_2 treated WO_3 surface.

The fairly negative adsorption energies of atomic N and N_2 on O_t indicate that these reaction pathways are chemically favorable. Additionally, these adsorption energies are less than the adsorption energy of N_2 on O_t vacancies, as seen in *Table 2*, which suggests that experimental observations may find more O-N bonds rather than W-N bonds.

Indeed, in Figure 4 the peak at 401.1eV from Prof. He's experiments indicates that there are O-N bonds observed on the only N_2 plasma-treated WO_3 001 surface.

4. Potential Energy Surface with DeepMD

4.1. Methodology

I used the open-source DeepMD-kit[7] framework that uses deep neural networks (DNNs) to train and create our model. The DNN takes both angular and radial atomic configurations into account while fitting the data. Not only can it use the distance between atoms as input, but also

[7] Han Wang, Linfeng Zhang, Jiequn Han, and Weinan E. "DeePMD-kit: A deep learning package for many-body potential energy representation and molecular dynamics." Computer Physics Communications 228 (2018): 178-184.

atomic local frame inputs. The main purpose of these descriptors is the aim to model and then predict the physics and interactions between atoms of different types in given training set systems (or other systems if the model is built to extrapolate).

To train the model, additional DFT data was used to train the model. The model was trained with data from ab initio molecular dynamics (AIMD) simulations and optimizations involving initial configurations generated by Python scripts. These DFT calculations were performed by VASP with the Perdew-Burke-Ernzerhof (PBE) exchange-correlation (XC) functional, as mentioned in DFT Methods.

For the model, it is currently trained on 3394 geometries of a WO_3(vac) + N_2 system, 53 geometries of a WO3 + N system, and 61 geometries of a WO3 + N_2 system to experiment with DeepMD-kit. Ninety percent of the geometries were assigned to be training data, with the rest as validation data. The model was then trained for 1,000,000 steps, taking approximately 6 hours on an NVIDIA GPU partition. The learning rate of the process is an exponential decay, with the decay steps at 10,000 and the initial learning rate at 0.001, which yields the equation $lr = 0.001\, e^{-\frac{step}{10{,}000}}$. Additionally, the descriptor for this initial testing model is assigned to be *se_e2_a*, which is constructed of both angular and radial atomic confirmations and takes the distance between atoms as input for the neural network. The cut-off radius used is 7 Å. The model hidden layer sizes, in order, are 25, 50, 100, 100, and 100 with an axis neuron of 16. This model is referred to as *Model1*

Model1 was assessed with the validation data of systems WO_3 + N, WO_3 + N_2, and WO_3(vac) + N_2 to evaluate its performance in capturing the physics of the systems and extrapolation capabilities. This model was frozen and then used to run optimization simulations with LAAMPS[8] for two initial configurations containing WO_3 + N_2 and WO_3(vac) + N_2 for additional comparisons with DFT calculations.

To verify that the *se_e2_a* descriptor can be used for the model to learn the physics in systems involving N, W, and O species, I trained a model with the same configuration as above but only used data for the WO_3(vac) + N_2 system training data. Freezing this model and then using LAAMPS to minimize and test this model in a WO_3 + N_2 system, we found that the optimized structure resembled the final configuration from DFT calculations. Therefore, we proceeded with this descriptor for this project.

---

[8] LAMMPS - a flexible simulation tool for particle-based materials modeling at the atomic, meso, and continuum scales, A. P. Thompson, H. M. Aktulga, R. Berger, D. S. Bolintineanu, W. M. Brown, P. S. Crozier, P. J. in 't Veld, A. Kohlmeyer, S. G. Moore, T. D. Nguyen, R. Shan, M. J. Stevens, J. Tranchida, C. Trott, S. J. Plimpton, Comp Phys Comm, 271 (2022) 10817.

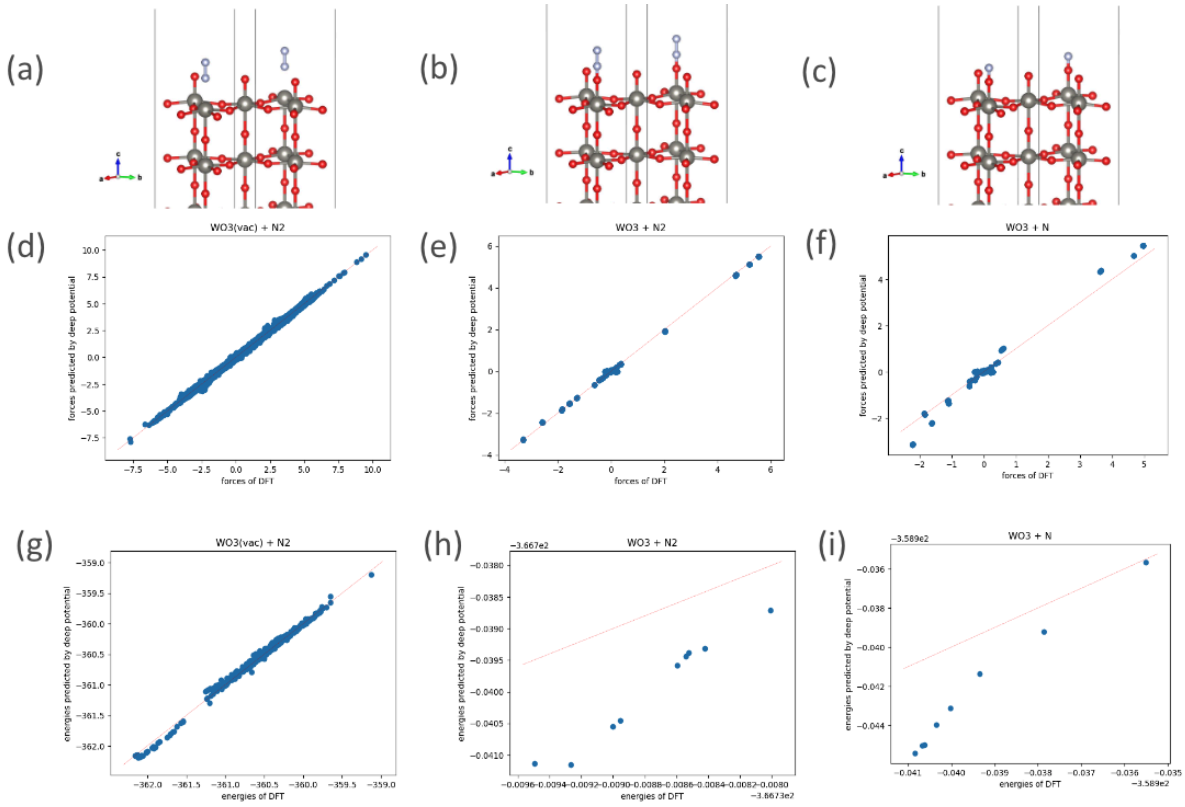

Figure 5. Comparison between energies and forces predicted by *Model1* and values from training data. The red line represents exact matches. (a) WO_3(vac) + N_2 system. (b) WO_3 + N_2 system. (c) WO_3 + N system. (d,e,f) Forces predicted by *Model1*. (g,h, i) Energies predicted by *Model1*. All the graphs' corresponding systems are the ones depicted in the same column it is found in.

Table 5. Energy and Force RMSEs of *Model1* in WO_3 + N_2 system validation data.

	WO_3(vac) + N_2	WO_3 + N_2	WO_3 + N
Energy RMSE (eV/Natom)	0.006994	0.00002557349	0.00006749
Force RMSE (eV/A)	0.05660	0.04169796	0.1732

4.2. Results and Discussion

Acceptable RMSE values in DNN validation systems that are similar to my project are typically less than 0.001 eV and 0.1 eV/A for energy and forces respectively. From *Table 5*, our values for the WO_3 (vac) + N_2 and WO_3 + N_2 systems meet these requirements, while the other one only meets the requirement for energy.

Figure 5 shows the comparison between energies and forces predicted by my model and energies from training data. For the first column (a,d,g) with the system WO_3(vac) + N_2, I find

that data points are not uniformly distributed among the force and energy spectrums, with most geometries clustered around 1.5 eV and -360.5 eV for energies and forces respectively. Despite this trend, the general adherence to the exact match line demonstrates the creation of a robust and accurate model for this specific system. For the non-vacany systems, in *Figure 5* the graphs for forces indicate a poor fit since most data points are extremely far from the exact match line.

I hypothesize that these discrepancies can be explained by the lack of training data for those two systems in comparison to the amount of data for the WO_3 (vac) + N_2 system. Due to how we set up our model with fitting energy taking priority over fitting forces, the model fits extremely well on a small amount of training data for the two non-vacancy systems for energy while for forces lacking the necessary amount to train well.

5. Summary

5.1. Conclusion

I studied the effects of H_2-plasma and N_2-plasma and water versus nitrogen interactions on hexagonal WO_3(001) surfaces via periodic DFT-PBE calculations. Specifically, I investigated the reaction pathway atomic H, a particle readily available with H_2-plasma, takes with the O_t surface to conclude that H_2-plasma aids more in the formation of terminating oxygen vacancies than room atmosphere through forming and desorbing H_2O. In addition, I explored the effects of coverage and temperature on the previously noted reaction pathway.

To investigate the reaction mechanisms of vibrational N_2 (N_2 (v)), I also trained a machine learning model on systems involving nitrogen species and WO_3(001) surfaces with and without vacancies. For systems that have large amounts of data, the fit is acceptable.

Thus, these DFT calculations are necessary for the quantitative and qualitative understanding of the interactions that will help the internal team I work with explain their experimental results and offer additional confidence in their findings.

5.2. Challenges and Setbacks

In the initial stages due to a programming error, we (my advisor and I) determined that the most stable termination for hexagonal WO_3(001) is the W-terminated side. However, once simulations were initially conducted and our hypothesis was challenged, I reviewed additional literature to find that the O-terminated side was the true stable surface.

Additionally, we found that including spin-polarization had a significant impact on the slab calculations after all calculations were finished and the report was written. I hypothesize that this is because of the asymmetry nature of the stoichiometric composition of WO_3, which causes the polarity to vary in the slab. This finding affected the accuracy of most to nearly all calculations involving the WO_3(001) slab by ±1-4 eV, which may explain the large magnitude of adsorption energy of atomic species on the surface.

5.3. Path Forward

I am aiming to finish the DFT simulations project by the end of August, and to do so involves re-submitting most configurations with spin-polarization included. I am in the process

of this at the moment. After the simulations are concluded, I will update this report for the internal team.

For the DNN, I aim to generate more training data and investigate the impact of different descriptors. In the process, the project will also be looked into through an automation lens, specifically using the Dp-Gen[9] package provided by Deepmd-kit's creators.

6. Acknowledgements

I thank Aditya, now Prof. Lele at Rowan University, for his help in guiding me through this Project by providing me with insightful resources, answering my questions, and doing much more as a mentor. I also thank Prof. Ju, who provided me with this opportunity to research alongside with other brightminded fellows. I would like to recognize Prof. He and other lab members for conducting experiments promptly and providing this project with valuable data. I also thank Princeton University for having me this summer.

[9] Yuzhi Zhang, Haidi Wang, Weijie Chen, Jinzhe Zeng, Linfeng Zhang, Han Wang, and Weinan E, DP-GEN: A concurrent learning platform for the generation of reliable deep learning based potential energy models, Computer Physics Communications, 2020, 107206.